States interpolating between number and coherent states and their interaction with atomic systems

2000 J. Phys. A: Math. Gen. 33 2231

(http://iopscience.iop.org/0305-4470/33/11/306)

J. Phys. A: Math. Gen. **33** (2000) 2231–2249. Printed in the UK PII: S0305-4470(00)07267-X

States interpolating between number and coherent states and their interaction with atomic systems

Hongchen Fu†, Yinqi Feng and Allan I Solomon

Quantum Processes Group, The Open University, Milton Keynes MK7 6AA, UK

E-mail: h.fu@open.ac.uk y.feng@open.ac.uk and a.i.solomon@open.ac.uk

Received 26 August 1999, in final form 25 January 2000

Abstract. Using the eigenvalue definition of binomial states we construct new intermediate number–coherent states which reduce to number and coherent states in two different limits. We reveal the connection of these intermediate states with photon-added coherent states and investigate their non-classical properties and quasiprobability distributions in detail. It is of interest to note that these new states, which interpolate between coherent states and number states, neither of which exhibit squeezing, are nevertheless squeezed states. A scheme to produce these states is proposed. We also study the interaction of these states with atomic systems in the framework of the two-photon Jaynes–Cummings model, and describe the response of the atomic system as it varies between the pure Rabi oscillation and the collapse–revival mode and investigate field observables such as photon number distribution, entropy and the Q-function.

1. Introduction

Since Stoler, Saleh and Teich proposed the binomial states (BS) in 1985 [1], so-called *intermediate* states which interpolate between some fundamental states such as number states, coherent and squeezed states and phase states have attracted much attention [2]. The BS are finite linear combinations of number states

$$|\eta, M\rangle = \sum_{n=0}^{M} \left[\binom{M}{n} \eta^n (1-\eta)^{M-n} \right]^{1/2} |n\rangle \tag{1.1}$$

where M is a non-negative integer, η is a *real* probability ($0 < \eta < 1$) and $|n\rangle$ is a number state of the radiation field. The photon number distribution is clearly a binomial distribution, whence the name *binomial state*. The BS are intermediate number–coherent states in the sense that they reduce to number and coherent states in different limits

$$|\eta, M\rangle \longrightarrow \begin{cases} |M\rangle & \eta \to 1 \\ |0\rangle & \eta \to 0 \\ |\alpha\rangle & \eta \to 0 \quad M \to \infty \quad \eta M = \alpha^2. \end{cases} \tag{1.2}$$

The BS also admit an eigenvalue definition [3]

$$\left(\sqrt{\eta} N + \sqrt{1-\eta}\sqrt{M-N}\, a \right) |\eta, M\rangle = \sqrt{\eta} M |\eta, M\rangle \tag{1.3}$$

† On leave of absence from the Institute of Theoretical Physics, Northeast Normal University, Changchun 130024, People's Republic of China.

0305-4470/00/112231+19$30.00

where a, $a^\dagger$ and N are the annihilation, creation and the number operators, respectively. The algebra involved is the $su(2)$ algebra (Holstein–Primakoff realization [4])

$$J^+ = \sqrt{M-N}\,a \qquad J^- = a^\dagger\sqrt{M-N} \qquad J^3 = \frac{M}{2} - N \tag{1.4}$$

and in the present case the coherent state limit is essentially the contraction of $su(2)$ to the Heisenberg–Weyl algebra generated by $a^\dagger$, a and 1.

Since number and coherent states are eigenstates of the number operator N and the annihilation operator a, respectively, it would seem more natural that, to define states interpolating between number and coherent states, we consider the eigenvalue equation of a linear combination of N and a itself (not J^+), namely,

$$\left(\sqrt{\eta}N + \sqrt{1-\eta}a\right)\|\eta,\beta\rangle = \beta\|\eta,\beta\rangle. \tag{1.5}$$

Here $0 < \eta < 1$ as before and β is an eigenvalue which will be determined not only from the eigenvalue equation (1.5) but also by a *physical requirement* (see section 2).

In this paper we study the states $\|\eta,\beta\rangle$ and their various properties. We find that for $\beta = \sqrt{\eta}M$ (M a non-negative integer), the solutions to equation (1.5) are indeed intermediate states which interpolate between number and coherent states. We also find that these states are closely related to the photon-added coherent states proposed by Agarwal and Tara [5]. The properties of this new state, such as their sub-Poissonian statistics, antibunching effects and squeezing effects, as well as their quasiprobability distributions (the Q- and Wigner functions), are studied in detail. Although coherent and number states are not squeezed, the new interpolating states are squeezed, and exhibit highly nonclassical behaviour. We also propose a scheme to produce these intermediate states in a cavity.

The intermediate number–coherent states are of particular interest in their interaction with atomic systems. In the context of the Jaynes–Cummings (JC) model, atomic population inversion exhibits two completely different phenomena: Rabi oscillation when the field is initially prepared in a number state; and periodic collapse and revival when the field is initially prepared in a coherent state. We naturally expect that the states proposed in this paper will present phenomena intermediate between Rabi oscillation and periodic collapse–revival, given that the initial state of the field is in an intermediate state. In section 6 we study the interaction of the states with the atomic systems based on the two-photon JC model and we indeed observe this intermediate behaviour. We also give an analytic derivation of the approximate photon number distribution of the field and find it exhibits strong oscillation at $\tau = \pi/4, 3\pi/4$ (τ is the scaled time). These phenomena are explained physically in terms of the entropy and Q-function of the field.

2. New intermediate number–coherent states

In this section we solve the eigenvalue equation (1.5), discuss the relation of the states (1.5) to photon-added coherent states and study the limit to number and coherent states.

2.1. Solutions

Expanding the state $\|\eta,\beta\rangle$ in number states

$$\|\eta,\beta\rangle = \sum_{n=0}^{\infty} C_n|n\rangle \tag{2.1}$$

inserting it into equation (1.5) and comparing the two sides of the equation, we find the solution of the eigenvalue equation (1.5):

$$\|\eta, \beta\rangle = C_0 \sum_{n=0}^{\infty} \frac{[\beta - \sqrt{\eta}(n-1)][\beta - \sqrt{\eta}(n-2)]\ldots\beta}{(\sqrt{1-\eta})^n \sqrt{n!}} |n\rangle \tag{2.2}$$

where C_0 is the normalization constant. Here, the eigenvalue β is an arbitrary complex number.

It is easy to see that for any complex number β the state (2.2) reduces to the coherent state $|\beta\rangle \equiv \mathrm{e}^{-\frac{|\beta|^2}{2}} \sum_{n=0}^{\infty} \frac{\beta^n}{\sqrt{n!}} |n\rangle$ in the limit $\eta \to 0$, as expected. However, it does not have a number state limit for arbitrary β since number states are eigenstates of N with non-negative integer eigenvalues. Further, we would like to have truncated states which are *finite* superpositions of the number states just as the binomial states are. With this in mind, we must choose $\beta = \sqrt{\eta}M$, where M is a non-negative integer. In this case it is easy to see that the coefficients C_n are truncated

$$C_n = \begin{cases} 0 & \text{when} \quad n > M \\ \left(\sqrt{\dfrac{\eta}{1-\eta}}\right)^n \dfrac{M!}{(M-n)!\sqrt{n!}} C_0 & \text{when} \quad n \leqslant M. \end{cases} \tag{2.3}$$

Here the normalization constant $C_0(\eta, M)$ is obtained as

$$C_0(\eta, M) = \left[\sum_{n=0}^{M} \left(\frac{\eta}{1-\eta}\right)^n \frac{(M!)^2}{[(M-n)!]^2 n!}\right]^{-\frac{1}{2}} = \frac{\lambda^M}{\sqrt{M! L_M(-\lambda^2)}} \tag{2.4}$$

where $\lambda \equiv \sqrt{(1-\eta)/\eta}$ and $L_M(x)$ is the Laguerre polynomial [6]

$$L_M(x) = \sum_{n=0}^{M} \frac{1}{n!} \binom{M}{M-n} (-1)^n x^n. \tag{2.5}$$

Inserting equations (2.3) and (2.4) into (2.1), we obtain the desired solution $\|\eta, (\beta = \sqrt{\eta}M)\rangle \equiv \|\eta, M\rangle$

$$\|\eta, M\rangle = \frac{1}{\sqrt{M! L_M(-\lambda^2)}} \sum_{n=0}^{M} \lambda^{M-n} \frac{M!}{(M-n)!\sqrt{n!}} |n\rangle \tag{2.6}$$

which is a *finite* linear superposition of number states.

We now consider the limiting cases of the above state (2.6) as number and coherent states. First consider the limit $\eta \to 1$. From the number-state expansion equation (2.6), it follows that

$$C_n = \frac{\lambda^{M-n} M!}{\sqrt{M! n!}(M-n)!} \longrightarrow \delta_{M,n} \tag{2.7}$$

namely, $\|\eta, M\rangle \to |M\rangle$. Then, in the different limit $\eta \to 0$, $M \to \infty$ with $\sqrt{\eta}M = \alpha$ a real constant, we have

$$\frac{M!}{(M-n)!} \to M^n \qquad \lambda^{-n} M^n \to \alpha^n \qquad C_0 \to \exp(-\alpha^2/2) \tag{2.8}$$

and therefore equation (2.6) reduces to the coherent state $|\alpha\rangle$.

The above discussion shows that the state $\|\eta, M\rangle$ may be considered as an intermediate state which interpolates between a number state and a coherent state.

2.2. Connection with photon-added coherent states

The state (2.6) can be written in more elegant form. By making use of $|n\rangle = \frac{a^{\dagger n}}{\sqrt{n!}}|0\rangle$, we can write equation (2.6) as

$$\|\eta, M\rangle = \frac{1}{\sqrt{M!L_M(-\lambda^2)}}\left[\sum_{n=0}^{M}\binom{M}{n}(a^\dagger)^n\lambda^{M-n}\right]|0\rangle = \frac{1}{\sqrt{M!L_M(-\lambda^2)}}(a^\dagger+\lambda)^M|0\rangle \tag{2.9}$$

where we have used the binomial formula.

Furthermore, thanks to the equation (real λ in our case)

$$D(-\lambda)a^\dagger D(\lambda) = a^\dagger + \lambda \tag{2.10}$$

where $D(\lambda)$ is the displacement operator

$$D(\lambda) = \exp[\lambda(a^\dagger - a)] \tag{2.11}$$

we can rewrite equation (2.9) in the form

$$\begin{aligned}\|\eta, M\rangle &= \frac{1}{\sqrt{M!L_M(-\lambda^2)}}D(-\lambda)a^{\dagger M}D(\lambda)|0\rangle \\ &= \frac{1}{\sqrt{M!L_M(-\lambda^2)}}D(-\lambda)a^{\dagger M}|\lambda\rangle \\ &\equiv D(-\lambda)|\lambda, M\rangle\end{aligned} \tag{2.12}$$

where $|\lambda\rangle = D(\lambda)|0\rangle$ is a coherent state and

$$|\lambda, M\rangle \equiv \frac{1}{\sqrt{M!L_M(-\lambda^2)}}a^{\dagger M}|\lambda\rangle \tag{2.13}$$

is a so-called *photon-added coherent state* or *excited coherent state* [5]. So from equation (2.13) we conclude that our new intermediate number–coherent states are *displaced excited coherent states*.

However, we would like to point out that our states are very different from the photon-added coherent states. The photon-added states are an *infinite* superposition of number states from M to infinity, while our states are a *finite* superposition of number states from 0 to M.

3. Nonclassical properties

In this section we shall investigate the statistical and squeezing properties of $\|\eta, M\rangle$, with special emphasis on the comparison with those of the BS.

3.1. Photon statistics

The easily derived relation

$$a^k\|\eta, M\rangle = \left[\frac{M(M-1)\ldots(M-k+1)L_{M-k}(-\lambda^2)}{L_M(-\lambda^2)}\right]^{1/2}\|\eta, M-k\rangle \tag{3.1}$$

for $k \leqslant M$ and $a^k\|\eta, M\rangle = 0$ for $k > M$, gives the mean value of $\langle N\rangle$ and $\langle N^2\rangle$

$$\langle N\rangle = \frac{ML_{M-1}(-\lambda^2)}{L_M(-\lambda^2)} \tag{3.2}$$

$$\langle N^2\rangle = \frac{M(M-1)L_{M-2}(-\lambda^2) + ML_{M-1}(-\lambda^2)}{L_M(-\lambda^2)} \tag{3.3}$$

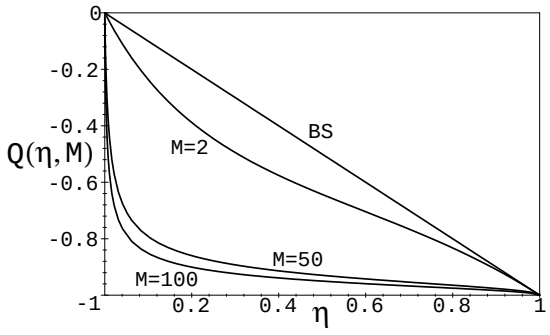

Figure 1. Mandel's Q-parameter for $M = 2, 50, 100$.

and Mandel Q-parameter [7]

$$Q(\eta, M) = \frac{\langle N^2\rangle - \langle N\rangle^2}{\langle N\rangle} - 1 = (M-1)\frac{L_{M-2}(-\lambda^2)}{L_{M-1}(-\lambda^2)} - M\frac{L_{M-1}(-\lambda^2)}{L_M(-\lambda^2)}. \tag{3.4}$$

If $Q(\eta, M) < 0$ (resp. $Q(\eta, M) > 0$), the field in the state $\|\eta, M\rangle$ is sub-Poissonian (resp. super-Poissonian). $Q(\eta, M) = 0$ corresponds to Poissonian statistics.

For a fixed M, there are two extreme cases: $\eta = 0$ (or $\lambda = \infty$) and $\eta = 1$ (or $\lambda = 0$). It is easy to see that

$$Q(\eta, M) \longrightarrow \begin{cases} -1 & \lambda = 0 \\ 0 & \lambda \to \infty \end{cases} \tag{3.5}$$

in agreement with the Q-parameter values for number states and the vacuum state. Here we have used the fact $L_M(0) = 1$ and $L_m(x)/L_n(x) \to 0$ for $m < n$ and $x \to \infty$.

Figure 1 is a plot of $Q(\eta, M)$ with respect to η for $M = 2, 50, 100$. The Q-parameter of the BS is also presented in the figure ($Q = -\eta$ for any M). From the figure we observe that the field in $\|\eta, M\rangle$ is *sub-Poissonian* except for the case $\eta = 0$.

We say that a field is antibunched if the second-order correlation function $g^{(2)}(0) = \langle a^\dagger a^\dagger a a\rangle/\langle a^\dagger a\rangle^2 < 1$ [8]. In fact, the occurrence of antibunching effects and sub-Poissonian statistics coincides for single-mode, time-independent fields such as the state $\|\eta, M\rangle$ of this paper. So the field $\|\eta, M\rangle$ is antibunched except at the point $\eta = 0$.

3.2. Squeezing properties

Define two quadratures x (coordinate) and p (momentum)

$$x = \frac{1}{\sqrt{2}}(a + a^\dagger) \qquad p = \frac{1}{\sqrt{2}\mathrm{i}}(a - a^\dagger). \tag{3.6}$$

Then we can easily obtain their variances $(\Delta x)^2 \equiv \langle x^2\rangle - \langle x\rangle^2$ and $(\Delta p)^2 \equiv \langle p^2\rangle - \langle p\rangle^2$

$$(\Delta x)^2 = \frac{1}{2} + \frac{ML_{M-1}(-\lambda^2)}{L_M(-\lambda^2)} + \frac{\lambda^2 L^{(2)}_{M-2}(-\lambda^2)}{L_M(-\lambda^2)} - 2\left[\frac{\lambda L^{(1)}_{M-1}(-\lambda^2)}{L_M(-\lambda^2)}\right]^2 \tag{3.7}$$

$$(\Delta p)^2 = \frac{1}{2} + \frac{ML_{M-1}(-\lambda^2)}{L_M(-\lambda^2)} - \frac{\lambda^2 L^{(2)}_{M-2}(-\lambda^2)}{L_M(-\lambda^2)} \tag{3.8}$$

where $L^{(k)}_m(x)$ is the associated Laguerre polynomial defined by [6]

$$L^{(k)}_m(x) = \sum_{n=0}^{m} \frac{(m+k)!}{(m-n)!n!(k+n)!}(-x)^n \qquad (k > -1). \tag{3.9}$$

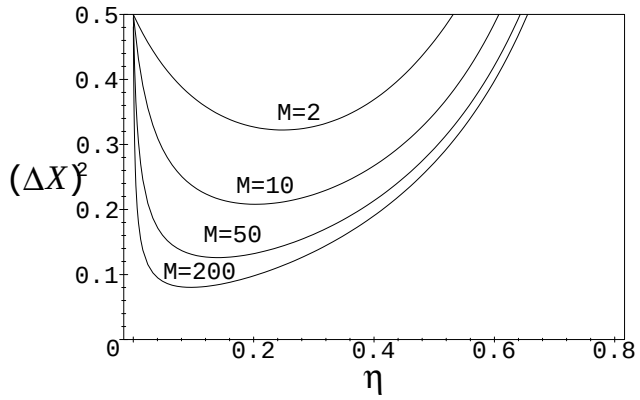

Figure 2. Variance $(\Delta x)^2$ of $\|\eta, M\rangle$ as a function of η for $M = 2, 20, 50$ and 200.

If $(\Delta x)^2 < \frac{1}{2}$ (or $(\Delta p)^2 < \frac{1}{2}$), we say the state is *squeezed* in the quadrature x (or p).

Figure 2 is a plot showing how the variance $(\Delta x)^2$ depends on the parameters η and M. When $\eta = 0$, $(\Delta x)^2 = \frac{1}{2}$ since the state is just the vacuum state and in this case the field is not squeezed. Then, as η increases the field becomes squeezed until maximum squeezing is reached; then the squeezing decreases until it disappears at a point η_0 depending on M. We note that $\eta_0 < 1$ when $M > 0$ since $(\Delta x^2) = M + \frac{1}{2} > \frac{1}{2}$ when $\eta \to 1$.

We also observe from figure 2 that the larger M, the stronger the squeezing, and the wider the squeezing range.

It is known that the optimal signal-to-quantum noise ratio for an arbitrary quantum state

$$\rho = \frac{\langle x\rangle^2}{(\Delta x)^2} \tag{3.10}$$

has the value $4N_s(N_s + 1)$ which is attainable for the usual coherent squeezed state [9]. For a coherent state the maximal ratio is $4N_s$, where N_s is the mean value of the number operator N for the quantum state.

For the intermediate number–coherent state $\|\eta, M\rangle$, the signal-to-quantum noise ratios for different parameters η and M are shown in figure 3. The ratio for $\eta = 0$ and $\eta = 1$, which correspond to the vacuum state and number state, respectively, is zero. For other η, we find from figure 3(*a*) that the larger M, the larger the ratio. Figure 3(*b*) gives plots of $4\langle N\rangle(\langle N\rangle + 1)$ ($\langle N\rangle$ is given by equation (3.2)), $4\langle N\rangle$ and the ratio for the state $\|\eta, M\rangle$ with $M = 10$. We find that:

(1) the ratio for $\|\eta, M\rangle$ is always smaller than the value $4\langle N\rangle(\langle N\rangle + 1)$, which is in accord with the general result [9];
(2) for some values of η the ratio is larger than $4\langle N\rangle$. We observe that the states with ratio larger than $4\langle N\rangle$ correspond to squeezed states (see figure 2).

4. Quasiprobability distributions

Quasiprobability distributions [10] in the coherent state basis turn out to be useful measures for studying the nonclassical features of radiation fields. In this section we study the Q-function (also called the Husimi function) and the Wigner function of the state $\|\eta, M\rangle$.

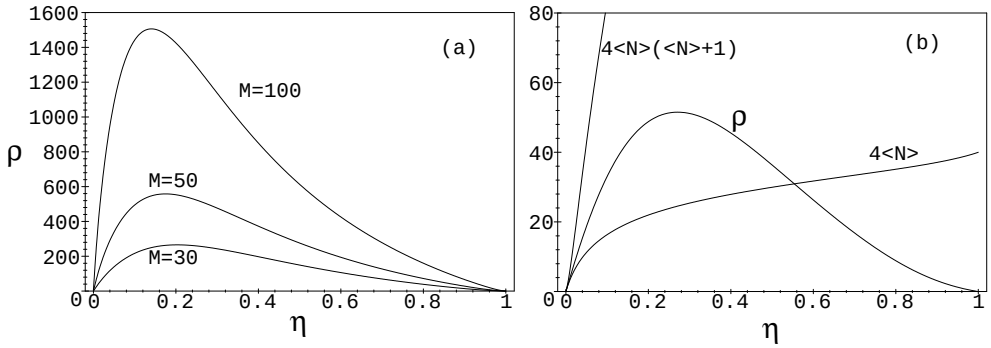

Figure 3. The signal-to-quantum noise ratio for $\|\eta, M\rangle$. (*a*) The ratio for different M; (*b*) comparison of ρ, $4\langle N\rangle(\langle N\rangle + 1)$ and $4\langle N\rangle$ for $M = 10$.

One can prove that (see appendix A), if two states $|\psi\rangle_\alpha$ and $|\psi\rangle$ satisfy $|\psi\rangle_\alpha = D(\alpha)|\psi\rangle$, where $D(\alpha) = \mathrm{e}^{\alpha a^\dagger - \alpha^* a}$ is the displacement operator, the Q- and Wigner functions of $|\psi\rangle_\alpha$ are simply a displacement of those of $|\psi\rangle$, namely

$$Q(\beta)_{|\psi\rangle_\alpha} = Q(\beta - \alpha)_{|\psi\rangle} \qquad W(\beta)_{|\psi\rangle_\alpha} = W(\beta - \alpha)_{|\psi\rangle}. \tag{4.1}$$

So the Q-function and the Wigner function of the state $\|\eta, M\rangle$ are easily obtained from those of the photon-added coherent states given in [5]

$$Q(\beta) = |\langle\beta\|\eta, M\rangle|^2 = \frac{\mathrm{e}^{-|\beta|^2}|\lambda + \beta|^{2M}}{M!L_M(-\lambda^2)} \tag{4.2}$$

$$W(\beta) = \frac{2(-1)^M L_M(|2\beta + \lambda|^2)}{\pi L_M(-\lambda^2)} \exp(-2|\beta|^2). \tag{4.3}$$

The Q-function equation (4.2) has a $2M$-fold zero at the position $\beta = -\lambda$, which signals the nonclassical behaviour†. These zeros are related to the negative parts of the Wigner function, since the Q-function can be defined as a smoothed Wigner function. Figure 4 gives plots of the Wigner function of $\|\eta, M\rangle$ for $M = 3$ and different η. One can clearly see the negative parts, except for the case $\eta = 0$ which corresponds to the vacuum state whose Wigner function is simply a Gaussian centred at the origin. As η increases from 0, the Gaussian distribution continuously deforms to the Wigner function of the number state $|3\rangle$.

We can also study squeezing properties from the Q-function by examining the deformation of its contours. Figure 5 is the contour plot of Q-functions for $M = 10$ and different η. We see that, when we increase η, the contour is squeezed in the x direction until a maximum squeezing is reached. Then the contour deforms to the shape of a banana, which occupies a wider range in the x direction and the squeezing is reduced. Finally, we obtain a circular contour for larger η corresponding to no squeezing (cf figure 2).

5. Generation of intermediate states

The main difference between the intermediate states described herein and photon-added coherent states is that the former are a *finite* superposition of number states. This suggests the possibility of an experiment to produce these states using the method proposed in [11].

† We thank the referee for this remark.

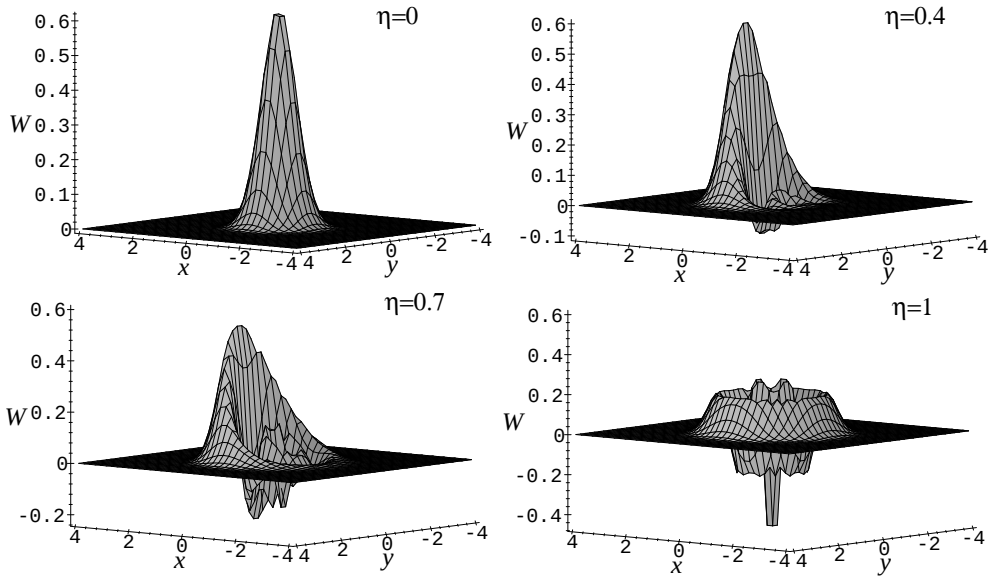

Figure 4. Wigner function of $\|\eta, M\rangle$ for $M = 3$ and $\eta = 0.1, 0.4, 0.7$ and 1. $\alpha = x + \mathrm{i}y$.

We can also generate the state $\|\eta, M\rangle$ by using the interaction of a photon and a two-level atom with an external classical driving field A in a cavity. In the rotating wave approximation, the Hamiltonian ($\hbar = 1$) is

$$\begin{aligned} H &= H_0 + V \\ H_0 &= \omega N + A(a^\dagger + a) + \tfrac{1}{2}\omega_0\sigma_3 \\ V &= g(a^\dagger\sigma_- + a\sigma_+) \end{aligned} \tag{5.1}$$

where $\sigma_3 = |e\rangle\langle e| - |g\rangle\langle g|$, $\sigma_+ = |e\rangle\langle g|$ and $\sigma_- = |g\rangle\langle e|$ are atomic operators, g is the one-photon coupling constant, ω_0 and ω are the atomic transition frequency and cavity resonant mode frequency, respectively, and we take the driving field A to be real and constant. The interaction Hamiltonian is

$$H_I(t) = U_0^{-1}(t)VU_0(t) \qquad U_0(t) = \mathrm{e}^{-\mathrm{i}H_0t} = \mathrm{e}^{-\mathrm{i}/2\omega tN - \mathrm{i}At(a^\dagger + a)}\mathrm{e}^{-\mathrm{i}\omega_0 t\sigma_3}. \tag{5.2}$$

Using the following relation (see appendix B):

$$U_0^{-1}(t)aU_0(t) = \mathrm{e}^{-\mathrm{i}\omega t}D(-A/\omega)aD(A/\omega) \tag{5.3}$$

where $D(A/\omega)$ is the displacement operator, we have

$$H_I(t) = gD(-A/\omega)(\mathrm{e}^{\mathrm{i}(\omega-\omega_0)t}a^\dagger\sigma_- + \mathrm{e}^{-\mathrm{i}(\omega-\omega_0)t}a\sigma_+)D(A/\omega). \tag{5.4}$$

Now we consider the on-resonance case, $\omega = \omega_0$. Then the interaction Hamiltonian is time-independent

$$H_I = gD(-A/\omega)(a^\dagger\sigma_- + a\sigma_+)D(A/\omega) \tag{5.5}$$

and therefore its time evolution operator is

$$U_I(t) = \mathrm{e}^{-\mathrm{i}H_It} = D(-A/\omega)\mathrm{e}^{-\mathrm{i}gt(a^\dagger\sigma_- + a\sigma_+)}D(A/\omega). \tag{5.6}$$

Suppose that the field is initially prepared in the vacuum state $|0\rangle$ and the atom in the excited state $|e\rangle$; namely, at $t = 0$, the system is in the state $|0\rangle \otimes |e\rangle$. At time t we have

$$U_I(t)|0\rangle \otimes |e\rangle = D(-A/\omega)\mathrm{e}^{-\mathrm{i}gt(a^\dagger\sigma_- + a\sigma_+)}D(A/\omega)|0\rangle \otimes |e\rangle. \tag{5.7}$$

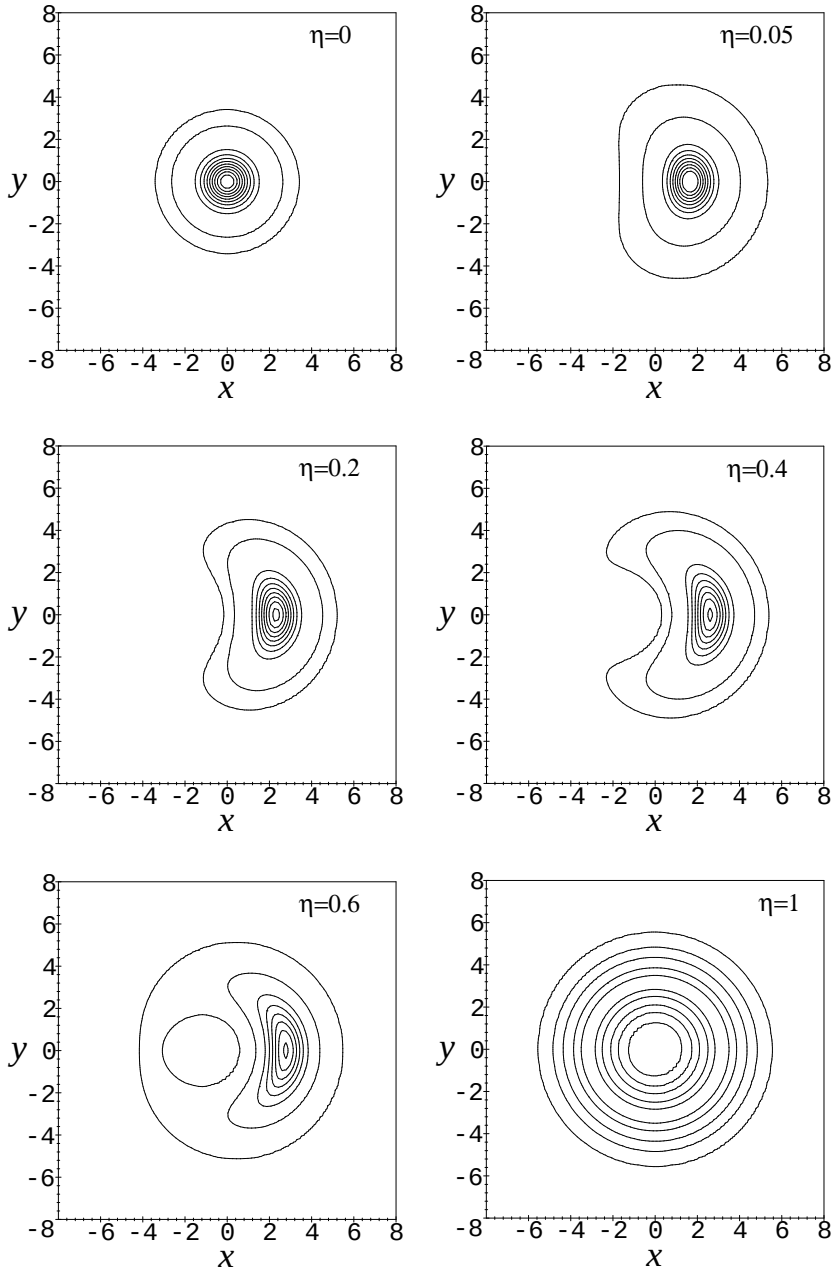

Figure 5. Contours of the Q-function of $\|\eta, M\rangle$. In all cases $M = 10$. $\alpha = x + \mathrm{i}y$.

When $gt \ll 1$, we have

$$U_I(t)|0\rangle \otimes |e\rangle = |0\rangle \otimes |e\rangle - \mathrm{i}gt[D(-A/\omega)a^\dagger D(A/\omega)|0\rangle] \otimes |g\rangle. \tag{5.8}$$

If the atom is detected in the ground state $|g\rangle$, the field is reduced to the state $\|\eta, 1\rangle$ with $\eta = \omega^2/(A^2 + \omega^2)$.

The state $\|\eta, M\rangle$ ($M > 1$) can be generated by a multiphoton generalization of the

Hamiltonian (5.1), namely, $V = g(a^{\dagger M}\sigma_- + a^M\sigma_+)$.

Note that the parameter A depends on the external driving field and is a tunable parameter. In particular, for large enough M, we can control the output state to be either a number or a coherent state by tuning the parameter A.

Finally, we may infer the presence of these new intermediate states to first order in an idealized nonlinear optics experiment. Consider a nonlinear Mach–Zehnder interferometer with a Kerr medium in one arm. The output state is the displaced Kerr state [12]

$$D(\xi)U_K(\gamma)|\lambda\rangle \qquad U_K(\gamma) \equiv \exp\left(\frac{\mathrm{i}}{2}\gamma a^{\dagger 2}a^2\right) \tag{5.9}$$

where $D(\xi)$ is the displacement operator and $\gamma \equiv 2\chi L/v$, L is the length of the Kerr medium, v the appropriate phase velocity inside the medium and χ the third-order susceptibility. When $\xi = -\lambda$, and γ is small enough, the above states can be approximated as

$$|0\rangle + \frac{\mathrm{i}}{2}\gamma\lambda^2\|\lambda, 2\rangle \tag{5.10}$$

showing the presence of the state $|\eta, 2\rangle$ in first order. In general, if we use a $(2S+1)$th-order nonlinear Kerr medium modelled in the interaction picture by [13]

$$H_{\mathrm{Kerr}} = \frac{\hbar\gamma_S}{(S+1)!}(a^\dagger)^{S+1}a^{(S+1)} = \frac{\hbar\gamma_S}{(S+1)!}N(N-1)\ldots(N-S) \tag{5.11}$$

we can find $\|\eta, M\rangle$ when γ_S is small enough.

6. Interaction with a two-level atomic system

In this section we turn to the interaction of the state $\|\eta, M\rangle$ with a simple two-level system in the framework of the two-photon JC model [14, 15] described by the following Hamiltonian ($\hbar = 1$):

$$H = \omega a^\dagger a + \tfrac{1}{2}\omega_0\sigma_3 + g(a^{\dagger 2}\sigma_- + a^2\sigma_+) = H_0 + V \tag{6.1}$$

with

$$H_0 = \omega a^\dagger a + \tfrac{1}{2}\omega_0\sigma_3 \qquad V = g(a^{\dagger 2}\sigma_- + a^2\sigma_+).$$

The notation is as in equation (5.1), but now g is the two-photon coupling constant for transition $|g\rangle \rightleftharpoons |e\rangle$. Suppose that, at the initial time $t = 0$, atom and field are decoupled and the atom is initially in the excited state $|e\rangle$, while the field is in the intermediate number–coherent state $\|\eta, M\rangle$. Then the combined atom–field wavefunction at time t is obtained as

$$\begin{aligned}|\psi_I(t)\rangle = &\sum_{n=0}^{M} C_n(\eta, M)[\cos(\delta_n t) - \mathrm{i}\frac{\Delta}{2\delta}\sin(\delta_n t)]\mathrm{e}^{\mathrm{i}\frac{\Delta}{2}t}|e\rangle \otimes |n\rangle \\ &-\mathrm{i}\sum_{n=0}^{M}\frac{\Omega_n}{\delta_n}C_n(\eta, M)\sin(\delta_n t)\mathrm{e}^{-\mathrm{i}\frac{\Delta}{2}t}|g\rangle \otimes |n+2\rangle\end{aligned} \tag{6.2}$$

where

$$\Omega_n = g\sqrt{(n+1)(n+2)} \qquad \delta_n = \sqrt{\frac{\Delta^2}{4} + \Omega_n^2} \qquad \Delta = \omega_0 - 2\omega. \tag{6.3}$$

For simplicity, we only consider the on-resonance interaction case $\Delta = 0$ as in [18] whereupon equation (6.2) simplifies to

$$|\psi_I(t)\rangle = \sum_{n=0}^{M} C_n(\eta, M)\cos(\Omega_n t)|e\rangle \otimes |n\rangle - \mathrm{i}\sum_{n=0}^{M} C_n(\eta, M)\sin(\Omega_n t)|g\rangle \otimes |n+2\rangle. \tag{6.4}$$

We now discuss some quantum characteristics of the system arising from the equation (6.4).

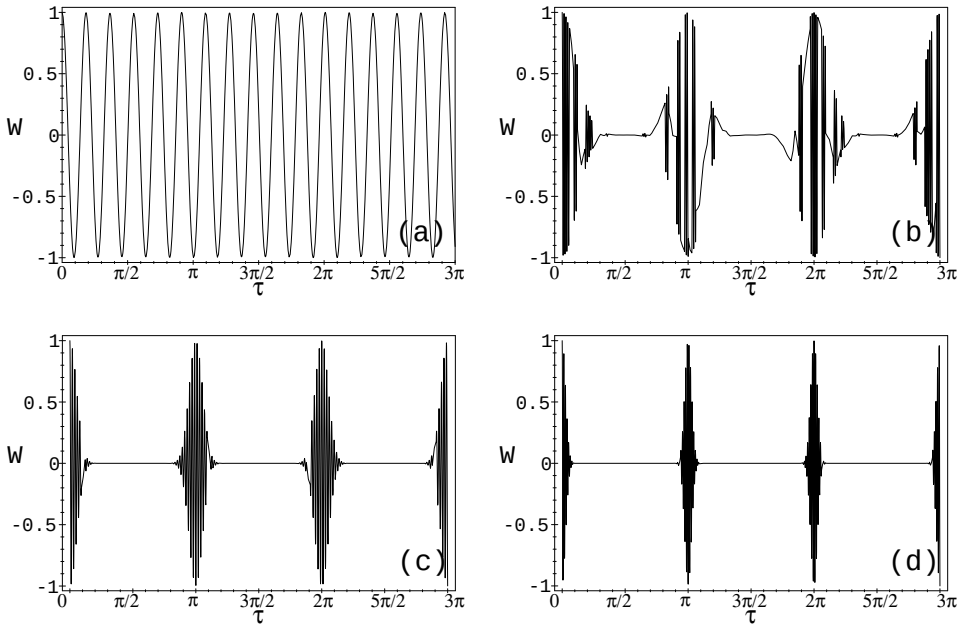

Figure 6. Atomic population inversion as a function of the scaled time τ. (*a*) $M = 4$, $\eta = 0.999$; (*b*) $M = 70$, $\eta = 0.8$; (*c*) $M = 70$, $\eta = 0.1$; (*d*) $M = 200$, $\eta = 0.001$.

6.1. Atomic population inversion

Atomic population inversion is an important atomic observable in the JC model and is defined as the difference between the probabilities of finding the atom in the excited state and in the ground state. From equation (6.4), the atomic population inversion is obtained as

$$W(t) = \langle \sigma_3 \rangle = \sum_{n=0}^{M} |C_n(\eta, M)|^2 \cos(2\Omega_n t). \tag{6.5}$$

Figure 6 gives the inversion versus scaled time $\tau \equiv gt$ for different M and η. From figure 6, we observe that the atomic population inversion exhibits the conventional Rabi oscillation for the M-number state limit ($\eta \to 1$). In fact, in the limit $\eta \to 1$, equation (6.5) is simplified as

$$W(t) = \cos(2\Omega_M t) \tag{6.6}$$

with frequency $2\Omega_M = 2g[(M+1)(M+2)]^{1/2}$ ($\approx 2Mg$ for high enough $\langle N \rangle$, see figure 6(*a*)). In the coherent state limit we observe the collapse–revival phenomenon, as we expect, with a revival time t_{cs} which can be estimated as π/g [18] for high enough $\langle N \rangle$ (that is, *revival frequency* $\Omega_{cs} \equiv 2\pi/t_{cs} \approx 2g$) (figure 6(*d*)). For the general intermediate case (figures 6(*b*) and (*c*)), remnants of both behaviour are seen; namely, an oscillation of frequency Ω_M modulated by the frequency Ω_{cs} with modulated amplitude dependent on the parameter η and M.

6.2. Field entropy

We now consider the cavity field observables, beginning with entropy which is a measure of the *amount of chaos* or lack of information about a system [16]. The entropy S of a quantum

mechanical system is defined as [17, 18]

$$S = -\operatorname{Tr}(\rho \ln(\rho))$$

where ρ is the density operator of the quantum system and the Boltzmann constant k is equal to unity. For a pure state, $S = 0$; otherwise $S > 0$, and it increases with increasing number of microstates with decreasing statistical weight.

In this section we study the time evolution of the field entropy in our system. Barnett and Phoenix [17] have proved that the field entropy S_f equals the atomic entropy S_a if the total initial state is a pure state. From equation (6.4) the atomic reduced density operator ρ_a can be easily obtained as

$$\rho_a \equiv \operatorname{Tr}_f(\rho) = \rho_{11}|g\rangle\langle g| + \rho_{12}|g\rangle\langle e| + \rho_{21}|e\rangle\langle g| + \rho_{22}|e\rangle\langle e| \tag{6.7}$$

where

$$\begin{aligned}
\rho_{11} &= \sum_{n=0}^{M} |C_n(\eta, M)|^2 \sin^2(\Omega_n t) \\
\rho_{22} &= \sum_{n=0}^{M} |C_n(\eta, M)|^2 \cos^2(\Omega_n t) \\
\rho_{12} &= \rho_{21}^* = \sum_{n=0}^{M-2} C_{n+2}(\eta, M) C_n(\eta, M) \cos(\Omega_{n+2} t) \sin(\Omega_n t).
\end{aligned} \tag{6.8}$$

Then the field and atomic entropy $S_a = -\operatorname{Tr}_a(\rho_a \ln(\rho_a))$ can be expressed as

$$S_f = S_a = -\pi_+ \ln(\pi_+) - \pi_- \ln(\pi_-) \tag{6.9}$$

where $\pi_\pm$ are eigenvalues of the atomic reduced field density operator ρ_a

$$\pi_\pm = \tfrac{1}{2}\left(1 \pm \sqrt{(\rho_{22} - \rho_{11})^2 + 4|\rho_{12}|^2}\right). \tag{6.10}$$

The field entropy S_f as a function of τ is presented in figure 7. It is clear that S_f is a periodic function of time and it exhibits the conventional oscillation for the M-number state limit. As in the case of coherent initial states, the field entropy during the time evolution is dynamically reduced to zero at revival time t_R which means the cavity field can be periodically found in pure states, and reaches a maximum at $t_R/2$ and falls quickly to a minimum at $\tau = \pi/4, 3\pi/4$. Furthermore, for the general intermediate case, the field entropy has more minima as shown in figures 7(*b*) and (*c*) due to the frequency modulation.

6.3. Q-function

The quasiprobability distribution Q-function is defined as [19]:

$$Q(\beta) = \frac{1}{\pi}\langle\beta|\rho_f|\beta\rangle$$

where $\rho_f = \operatorname{Tr}_a(\rho)$ is the field reduced density operator

$$\begin{aligned}
\rho_f = \sum_{m,n=0}^{M} & C_m(\eta, M) C_n(\eta, M)[\cos(\Omega_m t)\cos(\Omega_n t)|n\rangle\langle m| \\
& + \sin(\Omega_m t)\sin(\Omega_n t)|n+2\rangle\langle m+2|]
\end{aligned} \tag{6.11}$$

and $|\beta\rangle$ is the coherent state. So the Q-function of the cavity field is

$$Q(\beta) = \frac{\mathrm{e}^{-|\beta|^2}}{\pi}\left(\left|\sum_{n=0}^{M} \frac{\beta^{*n}}{\sqrt{n!}} C_n(\eta, M)\cos(\Omega_n t)\right|^2 + \left|\sum_{n=0}^{M} \frac{(\beta^*)^{n+2}}{\sqrt{(n+2)!}} C_n(\eta, M)\sin(\Omega_n t)\right|^2\right). \tag{6.12}$$

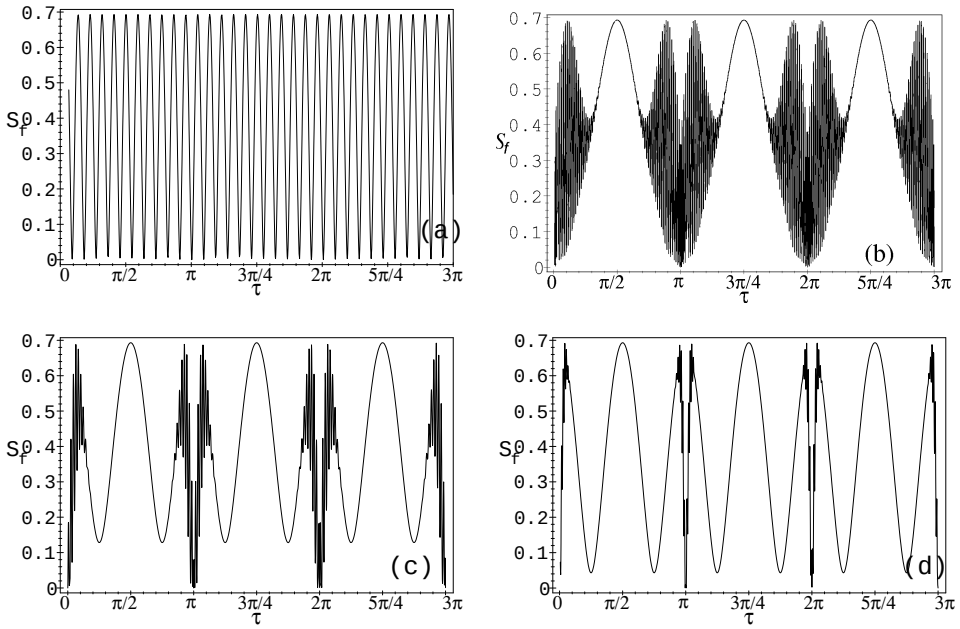

Figure 7. Entropy of the field as a function of scaled time τ. (*a*) $M = 4$ and $\eta = 0.9999$ (the initial field state is the number state $|4\rangle$); (*b*) $M = 70$ and $\eta = 0.8$; (*c*) $M = 70$ and $\eta = 0.1$; (*d*) $M = 200$ and $\eta = 0.005$.

In figure 8 we give contour plots of the Q-function at different times τ for $\eta = 0.1,\ 0.8$. At time $\tau = 0$, the Q-function has only a single peak and the field is in the pure quantum state $|\eta, M\rangle$ (cf figure 5). With the development of time, the Q-function begins to separate into two peaks. The smaller η, the faster the seperation. At time $\tau = \pi/2$, the Q-function exhibits the most separation and the field is in a mixed state since the entropy reaches its maximum. Then two peaks begins to merge together and finally combine in a single peak at time $\tau = \pi$, where the field is in a pure state with vanishing entropy.

6.4. Photon number distribution

The photon number distribution $P_n(t)$ of the field described by the reduced density matrix ρ_f is given by

$$P_n(t) = \langle n|\rho_f|n\rangle. \tag{6.13}$$

Inserting equation (6.11) into (6.13) we find the photon number distribution at time t

$$P_n(t) = |C_n(\eta, M)|^2 \cos^2(\Omega_n t) + |C_{n-2}(\eta, M)|^2 \sin^2(\Omega_{n-2} t). \tag{6.14}$$

Figure 9 shows the behaviour of the photon number distribution at times $\tau = 0, \pi/4, \pi/2, 3\pi/4$ and π. From these figures we can observe that the photon number distribution exhibits strong oscillation at time $\tau = \pi/4$ and $3/4\pi$ for the intermediate states. In fact, at those times, the field is a superposition of two components (see figure 8) and its entropy decreases rapidly to a minimum (see figure 7). Partial interference between two component results in strong oscillation of the photon number distribution. However, the oscillation is not *perfect* (see below). Nevertheless, it is perfect at the slightly earlier time $\tau = \pi/4 - \xi$ (see the dashed curves in figures 9(*a*) and (*b*)).

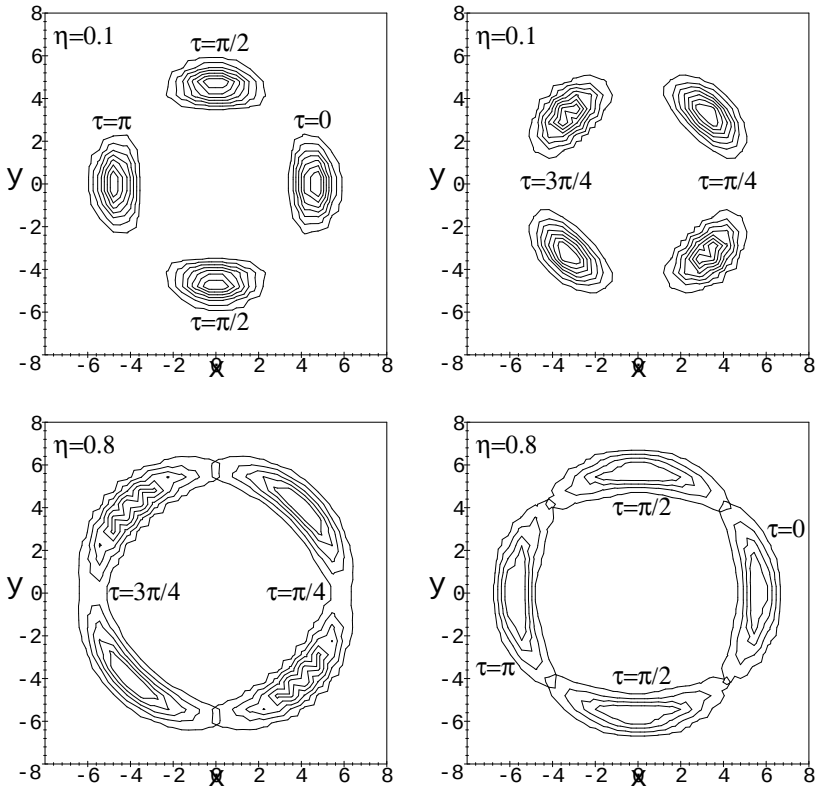

Figure 8. Contour plots of the Q-function of the field at $\tau = 0, \pi/4, \pi/2, 3\pi/4$ and π. Here we choose $\eta = 0.1, 0.8$.

This effect is not hard to understand. In fact, at $\tau = \pi/4$, we have the following approximate result (see appendix C):

$$P_n(t) = \left[1 + \frac{(1-\eta)^2 n(n-1)}{\eta^2 (M-n+2)^2 (M-n+1)^2}\right] |C_n(\eta, M)|^2 \sin^2 \left[\left(n - \frac{1}{2}\right)\tau\right]_{\tau=\frac{\pi}{4}} \tag{6.15}$$

for the high enough $\langle N \rangle$ case. Equation (6.15) is a strongly oscillating function which explains the large oscillations of the photon number distribution. However, due to the additional term $\tau/2 = \pi/8$, the function $\sin^2[(n - \frac{1}{2})\tau]_{\tau=\pi/4}$ cannot be zero for any integer n; in other words, the oscillation is not perfect. However, $P_n(t)$ is zero at the slightly earlier time $\tau = \pi/4 - \xi$, where ξ is chosen to make $(n - \frac{1}{2})\tau$ a multiple of π.

From figure 9(c) we also observe that the photon number distribution at $\tau = \pi$ is simply a displacement by 2 from that at the time $\tau = 0$. For the large photon number case, this fact can be proved analytically. Using equation (C.4) in appendix C, we have

$$\sin(\Omega_{n-2} t) \approx \sin(n\pi - \pi/2) = (-1)^{n+1}$$

$$\cos(\Omega_n t) \approx \cos[(n+1)\pi + \pi/2] = 0.$$

So the photon number distribution (6.14) at $\tau = \pi$ becomes

$$P_n(\pi/g) = |C_{n-2}(\eta, M)|^2 \equiv P_{n-2}(0). \tag{6.16}$$

In the same way we find that, at $\tau = \pi/2$, the photon number distribution is

$$P_n(\pi/2g) = \tfrac{1}{2}(|C_n(\eta, M)|^2 + |C_{n-2}(\eta, M)|^2) = \tfrac{1}{2}(P_n(0) + P_n(\pi/g)) \tag{6.17}$$

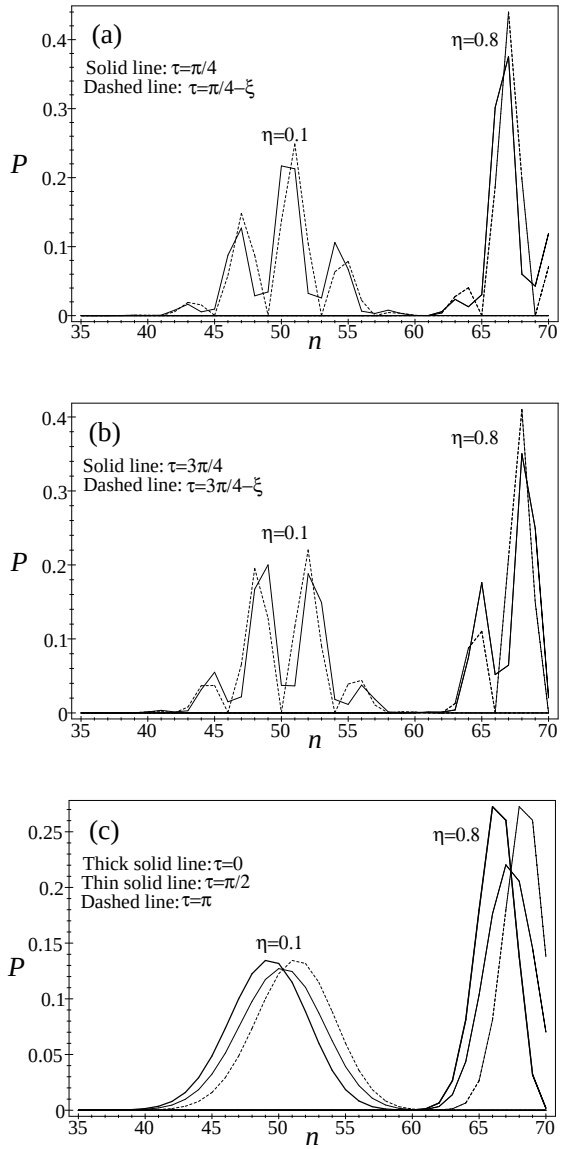

Figure 9. Number distribution of the photon field at different times: $\tau = 0, \pi/4, \pi/2, 3\pi/4$ and π for $\eta = 0.1, 0.8$. In (*a*) and (*b*) we also present the distribution at a slightly earlier time $\tau - \xi$, where ξ is chosen as $\frac{1}{140}$ and $\frac{1}{180}$ for $\eta = 0.1$ and $\eta = 0.8$, respectively.

namely, the *average* of the photon number distributions at $\tau = 0$ and $\tau = \pi$. In figure 9(*c*) this fact can be clearly observed.

7. Conclusion

In this paper we have described new states $\|\eta, M\rangle$ which interpolate between number and coherent states and have investigated their various properties. Unlike photon-added coherent

states, to which they are related, these states are a *finite* superposition of number states. We also analysed the limiting cases $\eta \to 1$ and $\eta \to 0$, $M \to \infty$ corresponding to number and coherent states, respectively. Salient statistical properties of $\|\eta, M\rangle$ such as the sub-Poissonian distribution, the anti-bunching effect and the squeezing effects were investigated for a wide range of parameters. The nonclassical features of thse states for certain parameter ranges were demonstrated in terms of the quasiprobability distributions, the Q- and Wigner functions. We also proposed an experiment to generate these states, inferring their presence in certain nonlinear systems.

We then considered the interaction of these interpolating number–coherent states with a two-level atomic system, exemplified by the two-photon JC model. We first studied the dynamics of atomic population inversion. On an intuitive level, one expects that the response of the atomic system will vary between the Rabi oscillation typical of an initial number state, and the collapse–revival mode for an initial coherent state; and indeed this is what one obtains. We found that it exhibited the conventional Rabi oscillation for the M-number state limit with frequency Ω_M ($\approx 2Mg$) and the collapse–revival phenomenon for the coherent state limit with revival frequency $\Omega_{\rm cs} \approx 2g$. For the general intermediate case, remnants of both behaviour were seen; namely, an oscillation of frequency Ω_M modulated by the frequency $\Omega_{\rm cs}$ with modulated amplitude dependent on the parameter η and M.

We further investigated the field observables, the entropy, Q-function and photon number distribution. It is of interest that the photon number distribution exhibits strong oscillation at $\tau = \pi/4, 3\pi/4$. At those times, the field entropy falls rapidly to a minimum and the Q-function separates into two peaks, which means that the field is a superposition of almost pure states and interference between components of the superposition state leads to strong oscillation of the photon number distribution. An approximate analytical solution is presented to explain this result.

The remarkable properties of these intermediate number–coherent states provide a useful tool for theoretical investigation of model systems; their generation by nonlinear systems tempts us to believe that the states found in this paper may play an important role in quantum optics.

Acknowledgments

H Fu is supported in part by the National Natural Science Foundation of China. We would like to thank Dr A Greentree of the Quantum Processes Group of the Open University for enlightening discussion on the production of these states, and the referee for valuable comments.

Appendix A. Displaced quasiprobability distributions

For the Q-function, we prove equation (4.1) as follows:

$$\begin{aligned} Q(\beta)_{|\psi\rangle_\alpha} &= |\langle\beta|D(\alpha)|\psi\rangle|^2 = |\langle 0|D(-\beta)D(\alpha)|\psi\rangle|^2 \\ &= |\langle\beta-\alpha|\psi\rangle|^2 = Q(\beta-\alpha)_{|\psi\rangle} \end{aligned} \tag{A.1}$$

where we have used the relation

$$D(\delta)D(\gamma) = D(\delta+\gamma)\mathrm{e}^{\frac{1}{2}(\delta\gamma^*-\gamma\delta^*)} = D(\delta+\gamma)\mathrm{e}^{\mathrm{i}\mathrm{Im}\,(\delta\gamma^*)} \tag{A.2}$$

for arbitrary complex numbers δ and γ. From the following definition of the Wigner function [20]:

$$W(\beta) = \frac{2}{\pi}\sum_{k=0}^{\infty}\langle\beta, k|\rho|\beta, k\rangle \tag{A.3}$$

where $|\beta, k\rangle \equiv D(\beta)|k\rangle = \mathrm{e}^{\beta a^\dagger - \beta^* a}|k\rangle$ is the displaced number state ($|k\rangle$ is the number state) and $\rho = |\eta, M\rangle\langle\eta, M|$ is the density matrix of the states considered, we can prove the second relation in equation (4.1) in the same way as in the Q-function case.

Appendix B. Proof of formula equation (5.3)

In this appendix we give a proof of equation (5.3). We use the following formula:

$$\mathrm{e}^{-F} G \mathrm{e}^{F} = \sum_{n=0}^{\infty} \frac{(-1)^n}{n!} \underbrace{[F, [F, \ldots, [F}_{n \text{ copies}}, G] \ldots]]. \tag{B.1}$$

For the case in hand

$$F = -\mathrm{i}\omega t N - \mathrm{i}t A(a^\dagger + a) \qquad G = a. \tag{B.2}$$

It is easy to see that

$$\begin{aligned}
&[F, G] = \mathrm{i}\omega t a + \mathrm{i}At \\
&[F, [F, G]] = \mathrm{i}\omega t [F, G] \\
&[F, [F, [F, G]]] = \mathrm{i}\omega t [F, [F, G]] = (\mathrm{i}\omega t)^2 [F, G] \\
&\ldots \\
&\underbrace{[F, [F, \ldots, [F}_{n \text{ copies}}, G] \ldots]] = (\mathrm{i}\omega t)^n [F, G] \\
&\qquad = (\mathrm{i}\omega t)^n a + (\mathrm{i}\omega t)^n A/\omega = (\mathrm{i}\omega t)^n D(-A/\omega) a D(A/\omega)
\end{aligned} \tag{B.3}$$

where $D(A/\omega)$ is the displaced operator. Substituting equation (B.3) into equation (B.1) we obtain the formula equation (5.3).

Appendix C. Photon number distribution for large photon number

In this appendix we present an analytical treatment of the photon number distribution in the large photon number regime. The photon number distribution of the two-photon JC model with initial state $|e\rangle \otimes \sum_n C_n|n\rangle$ can be obtained as

$$P_n(t) = |C_n|^2 \cos^2\left(\sqrt{(n+1)(n+2)}\tau\right) + |C_{n-2}|^2 \sin^2\left(\sqrt{(n-1)n}\tau\right) \tag{C.1}$$

where $\tau = gt$ is the scaled time as before.

Here we only consider an initial field state which is narrower than that of a coherent state. For a distribution $\{|C_n|^2\}$ we can calculate the variance as

$$(n - \bar{n})^2 = \langle N^2 \rangle - \langle N \rangle^2. \tag{C.2}$$

For the coherent state $|\alpha\rangle$, we have $(n - \bar{n})^2 = \bar{n}$. So for highly excited coherent states where $\bar{n} \to \infty$, we have $n \sim \bar{n}$. In the following we only consider a distribution $\{|C_n|^2\}$ narrower than the Poisson distribution, namely

$$(n - \bar{n})^2 \leqslant \bar{n}. \tag{C.3}$$

So for large enough $\bar{n}$ we also have $n \sim \bar{n}$. In this case, we have

$$\begin{aligned}
&\sqrt{(n+1)(n+2)} \approx \sqrt{n^2 + 3n} = n\sqrt{1 + \frac{3}{n}} = n + \frac{3}{2} = \left(n - \frac{1}{2}\right) + 2 \\
&\sqrt{(n-1)n} = \sqrt{n^2 - n} = n\sqrt{1 - \frac{1}{n}} \approx n - \frac{1}{2}.
\end{aligned} \tag{C.4}$$

Futhermore, when $\tau = \pi/4$ we have

$$\cos^2\left(\sqrt{(n+1)(n+2)}\tau\right) = \cos^2\left[\left(n-\frac{1}{2}\right)\tau + \frac{\pi}{2}\right]_{\tau=\frac{\pi}{4}} = \sin^2\left[\left(n-\frac{1}{2}\right)\tau\right]_{\tau=\frac{\pi}{4}}. \tag{C.5}$$

Substituting equation (C.5) into equation (C.1) we obtain the approximate photon number distribution at $\tau = \pi/4$

$$P_n(t) = (|C_n|^2 + |C_{n-2}|^2)\sin^2[(n-\tfrac{1}{2})\tau]_{\tau=\frac{\pi}{4}}. \tag{C.6}$$

From equation (C.6) we find that, for the initial field whose photon distribution is narrower than a Poisson distribution, the photon number distribution at $\tau = \pi/4$ exhibits strong oscillation. However, $P_n(\pi/4)$ cannot be zero for any n due to the term $\tau/2 = \pi/8$ and the oscillation is not perfect. Nevertheless, the oscillation is perfect at a slightly earlier time $\tau = \pi/4 - \xi$, as indicated in [18] (for initial coherent state) and figures 9(*a*) and (*b*).

For coherent states we further have $|C_{n-2}|^2 \approx |C_n|^2$. So the photon number distribution is

$$P_n(t) = 2\mathrm{e}^{-\bar{n}}\frac{\bar{n}^n}{n!}\sin^2\left[\left(n-\frac{1}{2}\right)\tau\right]_{\tau=\frac{\pi}{4}} \tag{C.7}$$

which is simply the result given in [18].

Now we turn to the analytical approximate result (6.15). For the intermediate state, we can write the variance as

$$(n-\bar{n}_M)^2 = \langle N\rangle_{M-1}\langle N\rangle_M - \langle N\rangle_M^2 + \langle N\rangle_M \tag{C.8}$$

where $\bar{n}_M \equiv \langle N\rangle_M \equiv \langle \eta, M|N|\eta, M\rangle$. In general, we have $\langle N\rangle_{M-1} \leqslant \langle N\rangle_M \leqslant M$. For large enough $\bar{n}_M$, or M, we have $\langle N\rangle_{M-1} \approx \langle N\rangle_M$ and therefore $(n-\bar{n}_M)^2 \sim \bar{n}_M$ which leads to $n \sim \bar{n}_M$. So the result (C.6) is valid for the intermediate state case. Furthermore, the distribution $|C_n(\eta, M)|^2$ and $|C_{n-2}(\eta, M)|^2$ are related by

$$|C_{n-2}(\eta, M)|^2 = \frac{(1-\eta)^2 n(n-1)}{\eta^2(M-n+2)^2(M-n+1)^2}|C_n(\eta, M)|^2. \tag{C.9}$$

Substituting equation (C.9) into (C.6), we finally obtain (6.15).

Equation (C.4) can also be used to explain the behaviour of the photon number distribution at $\tau = \pi/2$ and π (see equations (6.16), (6.17) and figure 9).

References

[1] Stoler D, Saleh B E A and Teich M C 1985 *Opt. Acta* **32** 345
[2] Lee C T 1985 *Phys. Rev.* A **31** 1213
Barranco A V and Roversi J 1994 *Phys. Rev.* A **50** 5233
Baseia B, de Lima A F and da Silva A J 1995 *Mod. Phys. Lett.* B **9** 1673
Baseia B, de Lima A F and Marques G C 1995 *Phys. Lett.* A **204** 1
Fan H Y and Jing S J 1994 *Phys. Rev.* A **50** 1909
Fu H C 1997 *J. Phys. A: Math. Gen.* **30** L83 and references therein
[3] Fu H C and Sasaki R 1996 *J. Phys. A: Math. Gen.* **29** 5637
[4] Holstein T and Primakoff H 1940 *Phys. Rev.* **58** 1048
Katriel J, Rasetti M and Solomon A I 1987 *Phys. Rev.* D **35** 2601
[5] Agarwal G S and Tara K 1990 *Phys. Rev.* A **43** 492
[6] Gradshteyn I S and Ryzhik I M 1965 *Table of Integrals, Series and Products* (New York: Academic)
[7] Mandel L 1979 *Opt. Lett.* **4** 205
[8] See for example, Walls D F and Millburn G C 1994 *Quantum Optics* (Berlin: Springer)
[9] Yuen H P 1976 *Phys. Lett.* A **56** 105
Solomon A I 1994 *Phys. Lett.* A **188** 215
Feng Y and Solomon A I 1998 *Opt. Commun.* **152** 299

[10] Hillery M, O'Connel R F, Scully M O and Wigner E P 1984 *Phys. Rep.* **106** 121
[11] Janszky J, Domokos P, Szabo S and Adam 1995 *Phys. Rev.* A **51** 4191
[12] Wilson-Gordon A D, Bužek V and Knight P L 1991 *Phys. Rev.* A **44** 7647
[13] Gerry C C 1987 *Phys. Lett.* A **124** 237
Bužek V and Jex I 1989 *Acta Phys. Slov.* **39** 351
Paprzycka M and Tanaś R 1992 *Quantum Opt.* **4** 331
[14] Jaynes E T and Cummings F W 1963 *Proc. IEEE* **51** 89
[15] Shore B W and Knight P L 1993 *J. Mod. Opt.* **40** 1195
[16] Wehrl A 1978 *Rev. Mod. Phys.* **50** 221
[17] Barnett S M and Phoenix S J D 1989 *Phys. Rev.* A **40** 2042
[18] Bužek V and Hladký B 1993 *J. Mod. Opt.* **40** 1309
[19] Glauber R J 1963 *Phys. Rev.* **130** 2529
Glauber R J 1963 *Phys. Rev.* **131** 2766
[20] Moya-Cessa H and Knight P L 1993 *Phys. Rev.* A **28** 2479